To appear in *Review of Scientific Instruments*, 2005

Spectroscopy with Multichannel Correlation Radiometers

A.I. Harris
*Department of Astronomy, University of Maryland, College Park, MD 20742**

Correlation radiometers make true differential measurements in power with high accuracy and small systematic errors. This receiver architecture has been used in radio astronomy for measurements of continuum radiation for over 50 years; this article examines spectroscopy over broad bandwidths using correlation techniques. After general discussions of correlation and the choice of hybrid phase experimental results from tests with a simple laboratory multi-channel correlation radiometer are shown. Analysis of the effect of the input hybrid's phase shows that a 90° hybrid is likely to be the best general choice for radio astronomy, depending on its amplitude match and phase flatness with frequency. The laboratory results verify that the combination of the correlation architecture and an analog lag correlator is an excellent method for spectroscopy over very wide bandwidths.

I. INTRODUCTION

Modern analog lag correlators are capable of autocorrelation spectroscopy over wide bandwidths [1]. This article examines an application of analog lag correlators, that of measuring cross-correlation functions for spectroscopy with correlation detection techniques. Although variants of the correlation detection schemes are common for radio continuum radiometry, it seems that no one has yet adapted the architecture for spectroscopy (multichannel radiometry) for high-resolution spectroscopy with a single telescope. A cross-correlation spectrometer on a single-aperture instrument would have the same excellent stability as cross-correlation spectrometers in aperture synthesis arrays. In addition, as shown in Section IV, a multichannel correlation radiometer can share one analog cross-correlation backend spectrometer between two sky positions, providing a dual-beam system with about half the backend spectrometer cost and complexity of a receiver with dual total-power spectrometers.

Correlation radiometers have made accurate radio and millimeter-wave continuum intensity measurements of the radio sky, the Cosmic Microwave Background, of rapidly changing scenes, and polarimetry (e.g. [2–6]). A number of authors have described specific architectures and examined the operation and sensitivity of correlation radiometers in absolute terms and their suppression of effects from the $1/f$ noise common to amplifiers [4, 7–14]. In the following, Section II contains a general discussion of correlation and Section III gives an analysis of the choice of hybrid phase, information that is not readily available elsewhere. Section IV shows experimental results from tests with a simple laboratory multichannel correlation radiometer that verify the theoretical expectations.

*Electronic address: harris@astro.umd.edu

II. CORRELATION DETECTION

Ryle introduced correlation detection to radio astronomy with his invention of the phase-switching interferometer [15]. Ryle's interferometer squared the sum of the voltages from two antennas after modulating the phase of one antenna's signal. Maintaining phase sensitivity by multiplying voltages instead of detecting the total power alone made this a correlating instead of a phased array of antennas. Phase switching the signal from one antenna was the key element in the method's success, as it separated the desired cross-product of the two antenna's voltages from total power signals from the individual antennas. Correlation detection with rapid phase switching brought a substantial improvement in instrumental stability since gain and noise fluctuations of amplifiers on the two antennas were uncorrelated in time; the only correlated signal, that common to the two antennas, was from the astronomical source. Communication engineers [16, 17] had already recognized that correlation techniques were valuable for retrieving small periodic signals in noise, and eventually came to view cross-correlation as a method of producing an optimal filter: it selects the component of the input signal at one multiplier input with waveform equal to the reference signal at the other multiplier input [18]. Viewed in this light, synchronous detection is a familiar example of a correlation receiver.

Adding a four-port circuit (a "hybrid") to correlation detection combines signals from two regions of the focal plane of a single aperture telescope and redistributes them before amplification. This allows the correlation technique to be used for single-dish observations. Figure 1 shows the signal flow through a correlation radiometer; the components to the right of the hybrid are equivalent to a spatial interferometer's signal path. The terminology for correlation detection is unfortunately muddled. Communications engineers use the term correlation receiver to describe what radio astronomers usually think of as a spatial interferometer or a synchronous detector, while single-dish astronomical instruments take the name "correlation receiver" [10, 11] or the more apt "continuous comparison receiver" [4, 9]. More recently, the same

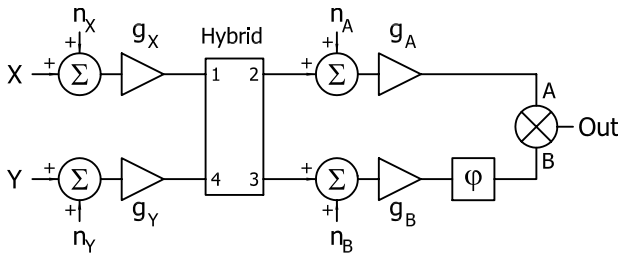

Figure 1: General model for a continuous comparison radiometer. The central block represents the input hybrid, with input ports numbered 1 and 4 and outputs 2 and 3. General noise and gain terms n and g and a phase shift φ complete the model.

architecture has been dubbed the "pseudo-correlation receiver," apparently based on a detail of the multiplier implementation.

Continuous comparison detection with a single-aperture telescope is the complement to the two-element spatial interferometer: an interferometer is sensitive to the correlated signals from two different regions of an aperture plane, while the continuous comparison radiometer extracts the uncorrelated part of the signals from two different regions of a focal plane. The input hybrid combines voltages from the source and reference positions in the focal plane, v_s and v_r, with different but known phase shifts before amplification. Cross-correlating the signals from the two amplifiers with the proper phase shift extracts the power difference between the two positions, $v_{out} \propto G\left(\langle v_s^2\rangle - \langle v_r^2\rangle\right)$, where the angle brackets denote an average over a time long compared with the reciprocal of the input bandwidth. The single-aperture continuous comparison radiometer has signal paths that are as similar as possible, so subsequent amplification and processing operate equally on the signals from both inputs. An amplifier gain fluctuation, for instance, has exactly the same effect on the signals from both positions in the focal plane. Correlated terms, including amplifier noise, average away with time as $1/\sqrt{B\tau}$, where B is the predetection bandwidth and τ is the integration time. With a differential measurement, gain fluctuations have no large noise term to amplify, greatly reducing the excess noise across the spectrum. Excess noise is a particular problem for instruments with wide bandwidths because the intrinsic measurement noise is proportional to $1/\sqrt{B}$ by the radiometer equation [19]. Fluctuations add noise in individual channels and instrumental structure across the spectrum.

A true differential measurement can greatly improve the stability of a radiometer compared with conventional total power measurements. Power amplification in a typical heterodyne radiometer is about 10^{12}, so it is not surprising that the most common limit to the stability of radiometric measurements is electronic and optical gain instability in time. Consider a total power radiometer with gain G, input source voltage v_s, and system noise voltage v_n. Its detector output voltage v_{out} is proportional to $G\langle v_{detector}^2\rangle$, or $v_{out} \propto G\left(\langle v_s^2\rangle + \langle v_n^2\rangle\right)$, plus the small uncorrelated cross term $2\langle v_s v_n\rangle$ that averages away with time as $1/\sqrt{B\tau}$. Spatial chopping and differencing between source and reference positions on the sky largely eliminates the relatively large noise signal on average, but even tiny fluctuations in system gain G or noise power $\langle v_n^2\rangle$ at the chop frequency can easily be much larger than the weak signal, $\Delta\big(G\langle v_n^2\rangle\big) \gg \langle v_s^2\rangle$, and can dominate the integrated signal. In contrast with Dicke's [19] scheme of sequential switching between astronomical and reference signals with a total power radiometer, the continuous comparison technique's simultaneous treatment of signal and reference positions provides a true differential measurement that greatly reduces the effects of time-variable gain fluctuations. Differencing without mechanically changing the optical system can also help reduce instabilities induced effects from microphonics or changing standing-wave structure that affect some types of receivers (e.g. local oscillator power modulation from a focal plane chopper or nutating secondary) and other low-level effects.

III. CHOICE OF HYBRID

Figure 1 defines the noise and gain variables for the following system analysis. Generalized noise voltages $n_{X,Y}$ and voltage gains $g_{X,Y}$ affect the voltages x and y at inputs X and Y. The hybrid's output is a phase-shifted mixture of its input voltages. Further equivalent noise voltages $n_{A,B}$ and voltage gains $g_{A,B}$ follow at each output. Noise voltages from components following the hybrid will be in phase and in quadrature (denoted I and Q) with the signal phase, so the noise terms are $n = n_I/\sqrt{2} + jn_Q/\sqrt{2}$, where $j = \sqrt{-1}$ and the total noise power is $\langle n^2\rangle = \langle n_I^2\rangle + \langle n_Q^2\rangle$. Solving for all noise and gain components in Fig. 1 is too messy to clearly show the circuit's properties. It is clearer to solve two basic cases, one with all gain and noise following an ideal hybrid and one with all preceding it. Nonideal effects are straightforward to include as modifications to these ideal cases.

Most astronomical continuous comparison radiometers incorporate a waveguide magic tee 180° hybrid [3, 13], although at least one has used a 90° quasi-optical hybrid [4], and good branch-line 90° hybrids now exist at frequencies to hundreds of gigahertz [20, 21]. The correlator's output has significantly different behavior for the 180° and 90° hybrids. A lossless hybrid's scattering matrix relates its output voltages to its input voltages, with ports numbered as in Figure 1, as:

$$\begin{bmatrix} v_{o1} \\ v_{o2} \\ v_{o3} \\ v_{o4} \end{bmatrix} = -j \begin{bmatrix} 0 & \beta & \alpha\, e^{j\theta} & 0 \\ \beta & 0 & 0 & -\alpha\, e^{-j\theta} \\ \alpha\, e^{j\theta} & 0 & 0 & \beta \\ 0 & -\alpha\, e^{-j\theta} & \beta & 0 \end{bmatrix} \begin{bmatrix} v_{i1} \\ v_{i2} \\ v_{i3} \\ v_{i4} \end{bmatrix}. \quad (1)$$

Here α and β are voltage coupling coefficients with $\alpha^2 +$

$\beta^2 = 1$. Zeros along the diagonal indicate that the ports are perfectly matched, and zeros on the cross-diagonal indicate no coupling between isolated ports. (A lossless hybrid must have these terms equal to zero to satisfy the unitary property of a lossless network S matrix [22].) The phase angle θ in Eq. (1) may vary arbitrarily in theory, with $\theta = 0$ and $\pi/2$ corresponding to realizable devices: the fully asymmetrical 180° and fully symmetrical 90° hybrids. Both have 180° phase total shifts between the outputs, but the shifts are distributed differently relative to the input signals.

Computing the multiplier output v_{out} is easiest when the signals are in complex phasor notation with implicit time dependence, $v(t) \equiv |v|e^{j\xi}$. Then the low frequency correlator output is $v_{out} \propto \langle \mathrm{Re}(v_A v_B^*) \rangle$ where $v_{A,B}$ are voltages at the multiplier input and the asterisk denotes the complex conjugate.

The most useful case has gain and noise following the hybrid. Solving for the multiplier's output shows that the interesting correlator power-difference signal $v_{out} \propto (\langle x^2 \rangle - \langle y^2 \rangle)$ is largest when a term $\cos(\zeta_A - \zeta_B - \varphi + \theta)$ is maximum. Here θ is the hybrid phase defined in Eq. (1), φ is an additional system phase shift shown in Fig. 1, and $\zeta_{A,B}$ are the gain phases $g_A g_B^* \equiv G e^{j(\zeta_A - \zeta_B)}$. Allowing for a phase deviation δ, ideally zero, from the maximum difference condition, this cosine term is maximum for $\varphi = \theta + \zeta_A - \zeta_B - \delta$. With that substitution the expressions become much simpler, and the multiplier output is

$$\begin{aligned} v_{out} \;\propto\; & \Big[\alpha\beta\left(\langle x^2\rangle - \langle y^2\rangle\right) + \left(\beta^2 - \alpha^2\right)\langle xy\rangle + \frac{1}{2}\Big(\langle n_{AI} n_{BI}\rangle + \langle n_{AQ} n_{BQ}\rangle\Big) \\ & + \frac{\alpha}{\sqrt{2}}\Big(\langle x n_{AI}\rangle - \langle y n_{BI}\rangle\Big) + \frac{\beta}{\sqrt{2}}\Big(\langle x n_{BI}\rangle + \langle y n_{AI}\rangle\Big)\Big] G\cos(\delta) \\ + \; & \Big[\frac{1}{2}\Big(\langle n_{AQ} n_{BI}\rangle - \langle n_{AI} n_{BQ}\rangle\Big) + \frac{\alpha}{\sqrt{2}}\Big(\langle x n_{AQ}\rangle + \langle y n_{BQ}\rangle\Big) \\ & + \frac{\beta}{\sqrt{2}}\Big(\langle x n_{BQ}\rangle - \langle y n_{AQ}\rangle\Big)\Big] G\sin(\delta) \end{aligned} \tag{2}$$

for a 180° hybrid ($\theta = 0$), and

$$\begin{aligned} v_{out} \;\propto\; & \Big[\alpha\beta\left(\langle x^2\rangle - \langle y^2\rangle\right) + \frac{1}{2}\Big(\langle n_{AQ} n_{BI}\rangle - \langle n_{AI} n_{BQ}\rangle\Big) \\ & + \frac{\alpha}{\sqrt{2}}\Big(\langle x n_{AI}\rangle - \langle y n_{BI}\rangle\Big) - \frac{\beta}{\sqrt{2}}\Big(\langle x n_{BQ}\rangle - \langle y n_{AQ}\rangle\Big)\Big] G\cos(\delta) \\ - \; & \Big[\left(\beta^2 + \alpha^2\right)\langle xy\rangle + \frac{1}{2}\Big(\langle n_{AI} n_{BI}\rangle + \langle n_{AQ} n_{BQ}\rangle\Big) \\ & + \frac{\alpha}{\sqrt{2}}\Big(\langle x n_{AQ}\rangle + \langle y n_{BQ}\rangle\Big) + \frac{\beta}{\sqrt{2}}\Big(\langle x n_{BI}\rangle + \langle y n_{AI}\rangle\Big)\Big] G\sin(\delta) \end{aligned} \tag{3}$$

for a 90° hybrid ($\theta = -\pi/2$).

Ideally, the correlator output contains only the power-difference term $\langle x^2 \rangle - \langle y^2 \rangle$. Other uncorrelated cross-terms (e.g. $\langle x n_A \rangle$) average to zero as $1/\sqrt{B\tau}$. Not all elements within the cross-terms will be completely uncorrelated in a practical system, with the correlated portions producing offsets at the correlator output. Fluctuations in system gain G (Eqs. 2 and 3) scale the offsets and can produce error terms that are large compared with the signal. An important goal for a continuous comparison radiometer is to keep the multiplier output near zero so the influence of gain fluctuations will be small. Minimizing the number and amplitude of correlator offsets is important to this end.

For ground-based radio astronomy the most important difference between the circuits with 180° and 90° hybrids is likely to be the response to cross-correlation in the input signals, $\langle xy \rangle$. Atmospheric emission in the telescope's near field and noise from the telescope's ohmic loss will provide correlated voltages between the two inputs. Suppressing this term requires either good hybrid amplitude balance or a flat system phase: at the correlator output this signal scales with $(\alpha^2 - \beta^2)$ for the 180° hybrid and $\sim \sin(\delta)$ for the 90° hybrid. A factor of ten suppression implies a hybrid power imbalance no worse than 0.45/0.55 (0.87 dB) or a maximum phase error term of $\sin(5.7°)$. Although it is difficult to build hybrids with tight amplitude matching across wide bands, wideband hybrids can have good phase flatness [20, 21]. If the other system components have good phase matching then the 90° hybrid would be the better choice.

Rejecting correlated input noise can also be useful when a common local oscillator signal (LO) is injected

before the hybrid. Injecting the LO into both ports with zero phase shift and equal amplitude will suppress noise in the oscillator's wings at the signal frequency. Injecting the LO into only one input port will pump both mixers but provides no LO noise rejection.

In any case, the 90° hybrid circuit always rejects correlated signals introduced after the hybrid better than the 180° hybrid circuit. These terms, with form $\langle n_{AQ} n_{BQ} \rangle$ and $\langle n_{AI} n_{BI} \rangle$, are suppressed by the $\sin(\delta)$ factor. Correlation in these terms can arise from bias fluctuations common to both gain paths or noise from the wings of a shared local oscillator (the noise and gain model implicit in Fig. 1 is generic and can include frequency conversion and multiple amplifiers).

For a nonideal hybrid, coupling between the output ports (2 and 3 in Fig. 2) is another important potential source of correlator offset. Noise radiated from, or signals reflected by, devices following the hybrid can emerge from the corresponding nominally isolated port to produce a correlated signal. A circulator following the hybrid can reduce the offset by an amount equal to the circulator isolation at the cost of adding loss before amplification. Lack of isolation between hybrid inputs is likely to be less of a problem since the signal reflected from the telescope or other optics is likely to be small. Further weak correlated terms will come from noise power emitted from the system and reflected back as an input signal (e.g. a fraction of n_A returns as input signal x to produce a nonzero $\langle x n_A \rangle$). This term is suppressed if the pathlength for the reflected signal is substantially longer than the correlation length, $l \simeq c/B$, where c is the speed of light.

Phase switching is a powerful method for removing correlator offsets and reducing the effects from nonideal colored noise. In comparison with amplitude modulation (Dicke switching) 180° phase switching is very efficient because the full signal amplitude is always present at the detector. Modulating the phase difference between the arms of a continuous comparison radiometer shifts the correlated signal output in frequency by an amount equal to the modulation frequency. Synchronous detection recovers the correlated signal while rejecting noise fluctuations at frequencies other than the modulation frequency. With phase switching before amplification, ideally just following the hybrid, a judicious choice of modulation frequency can remove much of the drift and $1/f$ noise associated with amplifier noise fluctuations. Since, to high order, any residual offsets or offsets from sources outside the phase modulation-demodulation boundaries are independent of the telescope's pointing, Dicke amplitude modulation by chopping on the sky (optically switching between two positions on the sky) and a final synchronous demodulation will largely remove the remaining offsets.

Phase switching does not suppress the direct effects of amplifier or multiplier gain or phase fluctuations, but symmetry can reduce their influence. Equations (2) and (3) show that the product of the voltage gains scales the input power difference as $G(\langle x^2 \rangle - \langle y^2 \rangle)$. A small gain fluctuation common to both chains introduces an amplitude error to the difference signal at the correlator output, but adds no error signal when the offsets are negligible. Multiplier gain fluctuations have the same effect as amplifier gain fluctuations in this case. The situation is different when the amplifier gain fluctuations are differential-mode instead of common-mode for the two amplifier chains. Faris [12] calculates the effect of a varying gain imbalance between the two chains for $g_2(f,t) = [1 + a(t)]g_1(f)$, where $g_{1,2}(f)$ are the complex amplifier voltage gains of the two chains and $a(t)$ is a zero-mean random variable that describes the differential-mode fluctuations. Fluctuations increase the output variance by a factor of $(1 + \langle a^2(t) \rangle)$ compared with the case of purely common-mode gain fluctuations between the two arms. Similar effects arise from differential phase fluctuations between the two arms. Strategies for minimizing differential-mode fluctuations could include biasing the amplifiers from a common power supply and keeping good thermal contact between corresponding parts of each chain.

The second case, with amplification preceding the hybrid's loss, is the obvious choice for maximizing the receiver sensitivity but negates much of the continuous comparison architecture's advantage. The maximum difference signal in this case is

$$\begin{aligned} v_{out} &= \alpha\beta\Big[\left(\langle x^2 \rangle |g_x|^2 - \langle y^2 \rangle |g_y|^2\right) \\ &\quad + \left(\langle n_x^2 \rangle |g_x|^2 - \langle n_y^2 \rangle |g_y|^2\right) \Big] , \end{aligned} \tag{4}$$

for both 180° and 90° hybrids. For this configuration to be useful nearly exact matching of both the noise power and power gains would be necessary. Slight imbalances in loss and gain will produce large offsets at the correlator output.

IV. SPECTROSCOPY WITH AN ANALOG LAG CROSS-CORRELATOR

Sensitive spectroscopy (multichannel radiometry) over broad bandwidths is important for observations of wide spectral lines from distant galaxies, searches for lines at with uncertain frequency, and measurements of pressure-broadened lines in planetary atmospheres. Spectrometer bandwidths can be tens of gigahertz with channel bandwidths of tens of megahertz. Such broad bandwidths place stringent requirements on system stability, so it is natural to pair wideband spectrometers with the continuous comparison architecture. Spectroscopy with a correlation radiometer requires measurement of the cross-correlation function over a range of time lag, or delay. Analog lag correlators use purely analog components to obtain the cross-correlation function $R_{AB}(\tau)$ as a function of lag τ:

$$R_{AB}(\tau) = \lim_{T \to \infty} \frac{1}{2T} \int_{-T}^{T} v_A(t) \cdot v_B(t+\tau)\, \mathrm{d}t \, . \tag{5}$$

Tapped transmission lines provide the time delays τ, transistor multipliers form the product of the two input voltages $v_A(t)$ and $v_B(t+\tau)$, and low-frequency electronics integrate the multiplier output to provide the time average.

A Fourier transform of the cross-correlation function yields the power density cross-spectrum. Transforming the correlation function to recover the spectrum is slightly more complicated than making a direct Fourier transform for analog correlators because the signal is not sampled at perfectly regular intervals. Although the mechanical spacing between the microwave signal taps along the transmission line is well defined by the traces on the circuit board, frequency-dependent component variations cause small erratic variations in the electrical delays between multipliers. A direct Fourier inversion to find the spectrum is not possible because the transform kernel's phase term cannot be reduced to a separable product of the delay time and frequency, as might be the case for simple line dispersion [1]. It is possible to correct the irregular sampling in software by measuring the spectrometer's response to a series of monochromatic signals at known frequencies, then expanding the astronomical input signal on these measured functions [1].

An interesting effect of this calibration scheme is that it defines the spectrometer's internal phase: by definition signals in phase with the calibration are real, and those with a relative 90° phase shift are imaginary. This property can be used to eliminate one of the phases in the usual complex cross-correlation measurement. When the calibration signals are injected at the radiometer's input the calibration and measured signals share the same phase shifts through the entire instrument, so the measured signal is purely real; the imaginary component contains only noise. A single cross-correlator can therefore measure the cross-correlation function. While purely real cross-correlations are unusual in most spectrometers, there is no fundamental reason that they cannot exist. A real correlation function has the convenient property of even symmetry in the lag domain, so the positive (or negative) lags alone contain all the necessary information to recover the spectrum. Although it is possible to build a full complex correlator and calibrate it at lower frequency, injecting the phase calibration signals at the input to the entire radiometer yields spectra at full spectral resolution with half the number of lags. This is not only a significant savings in spectrometer cost and complexity, but eliminates requirements on phase-matching between the two amplifier and processing chains. Digital correlators do not readily share this property because their topologies give them an intrinsic symmetry and phase related to the position of the zero-lag multiplier. A full complex correlator, or close phase matching across the receiver band, is needed for spectroscopy with a digital system and direct transform.

A simple laboratory continuous comparison radiometer, sketched in Figure 2, verifies that a WASP2 (Wideband Astronomical SPectrometer) analog lag correlator

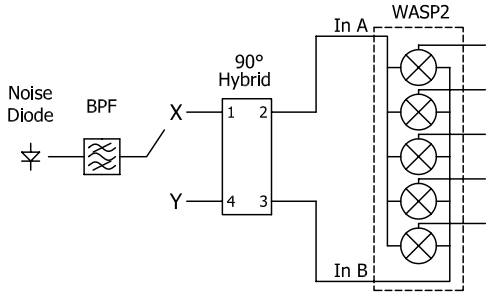

Figure 2: Block diagram of laboratory continuous comparison receiver test setup.

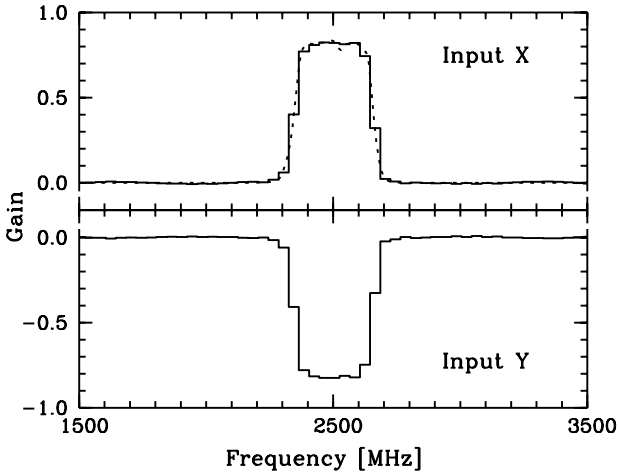

Figure 3: Spectra from the two inputs of a laboratory correlation radiometer with a WASP2 spectrometer configured as a cross-correlator. The dotted line is a network analyzer measurement of the filter transmission.

[1] properly produces power difference cross-spectra with this calibration scheme. The hybrid for the experiment was an off-the-shelf stripline 90° 2–4 GHz device. Cables lengths between the hybrid and cross-correlator brought the zero time-lag position close to one end of the multiplier ladder, for maximum spectral resolution, but were not otherwise trimmed for length or phase matching. A broadband noise diode and 300 MHz filter generated an artificial spectral line that could be connected to either hybrid input, denoted X and Y in Fig. 2. Phase calibration signals were fed into input X alone. Figure 3 shows that the spectrometer works as predicted. The artificial line at input X, with Y terminated, produces a positive spectral line, and the same signal at input Y, with X terminated, produces a negative spectral line. After removing the noise source's intrinsic spectral shape by dividing the raw spectra by spectra of the noise source alone, the filter center frequency, shape, and loss matched network analyzer measurements (Fig. 3). This confirms that the cross-correlation function is purely real. The sum of the two spectra is very close to zero. Residual phase errors scatter power across the spectrum at about 0.5% of

the peak line intensity, a well-understood dynamic range limit rather than a noise offset [1]. This fixed-pattern structure subtracts well with beamswitching.

These experimental results show that the combination of the continuous comparison architecture with a analog lag correlator is a very promising method for spectroscopy over very wide bandwidths.

Acknowledgments

The author thanks J. Kooi and T.G. Phillips for suggestions and several useful discussions about LO noise rejection and practical hybrid designs. The author also thanks the Caltech Submillimeter Group for their hospitality while this paper was written. This work was supported in part by grant AST-9819747 from the National Science Foundation.

[1] A. Harris and J. Zmuidzinas, Rev. Sci. Inst. **72**, 1531 (2001).
[2] C. Haslam, W. Wilson, D. Graham, and G. Hunt, Astron. Astrophys. Suppl. **13**, 359 (1974).
[3] N. Jarosik, C. Bennet, M. Halpern, G. Hinshaw, A. Kogut, M. Limon, S. Meyer, L. Page, M. Pospiezalski, D. Spergel, et al., Astrophys. J. Suppl. Ser. **145**, 413 (2003).
[4] C. Predmore, N. Erickson, G. Huguenin, and P. Goldsmith, IEEE Trans. Microwave Theory Tech. **MTT-33**, 44 (1985).
[5] K. Rholfs and T. Wilson, *Tools of Radio Astronomy* (Springer Verlag, 2000), chap. 4.5, 3rd ed.
[6] O. Koistinen, J. Lahtinen, and M. T. Hallikainen, IEEE Trans. Instrumen. Meas. **IM-51**, 227 (2002).
[7] R. Fano, *Signal to noise ratio in correlation detectors*, M.I.T. Res. Lab. Elec., Rep. RLE-186 (1951).
[8] S. Goldstein, Jr., Proc. IRE **43**, 1663 (1955), with further correspondence and errata in Proc. IRE **48**, 365, 1956.
[9] É.-J. Blum, Ann. Astrophys. **22**, 140 (1959).
[10] M. Tiuri, IEEE Trans. Antenn. Propag. **AP-12**, 930 (1964).
[11] R. Colvin, Ph.D. thesis, Stanford University (1961), also Stanford Radio Astronomy Institute Publ. No. 18A.
[12] J. Faris, J. Res. Nat. Bur. Stand.–C **71C**, 153 (1967).
[13] M. Seiffert, A. Mennella, C. Burigana, N. Mandolesi, M. Bersanelli, P. Meinhold, and P. Lubin, Astr. Astrophys. **391**, 1185 (2002).
[14] A. Mennella, M. Bersanelli, M. Seiffert, D. Kettle, N. Roddis, A. Wilkinson, and P. Meinhold, Astr. Astrophys. **410**, 1089 (2003).
[15] M. Ryle, Proc. R. Soc. Lon. A **211**, 351 (1952).
[16] Y. Lee, T. Chetham, and J. Wiesner, *The application of correlation functions in the detections of small signals in noise*, M.I.T. Res. Lab. Elec., Rep. RLE-141 (1949).
[17] Y. Lee and J. Wiesner, Electronics **23**, 86 (1950).
[18] P. Peebles, *Probability, Random Variables, and Random Signal Processes* (McGraw-Hill, 1993), p. 310, 3rd ed.
[19] R. Dicke, Rev. Sci. Inst. **17**, 268 (1946).
[20] S. Srikanth and A. Kerr, *Waveguide quadrature hybrids for ALMA receivers*, ALMA Memo 343 (2001), URL `http://www.alma.nrao.edu/memos/index.html`.
[21] J. Kooi, A. Kovacs, B. Bumble, G. Ghattopadhyay, M. Edgar, S. Kaye, H. LeDuc, J. Zmuidzinas, and T. Phillips, in *Millimeter and submillimeter detectors for astronomy II*, edited by J. Zmuidzinas, W. S. Holland, and S. Withington (SPIE–The International Society for Optical Engineering, 2004), vol. 4587 of *Proc. SPIE*, pp. 332–348.
[22] D. M. Pozar, *Microwave Engineering* (J.W. Wiley & Sons, 1998), pp. 354–357, 2nd ed.